



## Search for Diboson Production in $\cancel{E}_T + b\bar{b}$ channel at $\sqrt{s} = 1.96$ TeV

The CDF Collaboration  
URL <http://www-cdf.fnal.gov>  
(Dated: October 19, 2010)

Diboson production has been observed at the Tevatron using generic jets. Doing the same thing with heavy flavor jets is much more difficult. Here we attempt to measure the diboson cross-section specifically of  $WZ$  and  $ZZ$  events using a selection with large  $\cancel{E}_T$  and two  $b$  jets as an additional discriminant. Due to limited energy resolution we cannot distinguish between  $WZ$  and  $ZZ$  events so what we measure is a sum of these processes in our selection window. As no cut on the number of charged leptons in the event is performed, we are also sensitive to decays of the gauge bosons with  $e$ ,  $\mu$  or  $\tau$  leptons. We extract the signal from the background using the invariant mass distribution of the two jets in the event in a simultaneous fit of the region with no  $b$  tags and with two  $b$  tags. The extraction of the signal does not use the theoretical calculation of the  $V$ +jets integral cross section, whose invariant mass shape is cross-checked with  $\gamma$ +jets events from data, thereby considerably reducing the systematic uncertainty on the shape of this main background. We measure a cross section  $\sigma(p\bar{p} \rightarrow WZ, ZZ) = 5.0_{-2.5}^{+3.6}$  pb with a 95% CL limit  $\sigma < 13$  pb.

## I. INTRODUCTION

In this paper, we describe a measurement of the cross section for diboson production in a final state with  $\cancel{E}_T$  and  $b$ -tagged jets. Diboson production has been observed at the Tevatron in leptonic final states ( $WW$  - dilepton,  $WZ$ -trilepton,  $ZZ$  - four leptons). In the case of partially hadronic decay modes, we have observed a signal for combined measurement of  $WW$ ,  $WZ$  and  $ZZ$  in 3.5/fb, where the signal is dominated by  $WW$  [1]. In this paper, we describe a measurement where we apply  $b$  tagging to isolate the  $WZ$  and  $ZZ$  signals in the semi-leptonic decay channels. We use a double-fit to the invariant mass spectrum of di-jet pairs in events with two  $b$  tags and events with no  $b$ -tags. The signatures we are sensitive to are  $WZ \rightarrow \ell\nu b\bar{b}$  and  $ZZ \rightarrow \nu\nu b\bar{b}$  in the two-tag channel and all decays with  $\cancel{E}_T$  in the no-tag channel ( $WZ \rightarrow \ell\nu q\bar{q}, q\bar{q}'\nu\nu$  and  $ZZ \rightarrow \nu\nu q\bar{q}$ .)

The techniques developed for this measurement can be used in the search for a low-mass standard model Higgs boson produced in association with a gauge boson ( $WH \rightarrow \ell\nu b\bar{b}$ ,  $ZH \rightarrow \nu\nu b\bar{b}$ .)

## II. DATA SELECTION, BACKGROUNDS AND DATA SETS

We select events with two or more jets and  $\cancel{E}_T > 50$  GeV. The jets must have  $E_T > 20$  GeV and be within  $|\eta| < 2$ . The jets are required to have  $E_T > 20$  GeV and  $|\eta| < 2.0$ . The jet EM fraction of all jets with raw  $E_T > 10$  GeV has to be less than 0.9 such that electrons are not considered in the jet list. The  $\cancel{E}_T$  is corrected for jets and muons. To suppress the multi-jet contribution, we require the angle between the  $\cancel{E}_T$  vector and any identified jet above 5 GeV to be more than 0.4 radians.<sup>1</sup> Additionally, we require signed  $\cancel{E}_T$  significance to be more than 4 (see [1, 2]). Beam halo is removed by requiring the event EM fraction,  $E^{EM}/E^{TOT}$ , to be between 0.3 and 0.85. This event EM fraction is calculated based on energies of all jets with raw  $E_T > 10$  GeV. Since we apply  $b$ -tagging and allow for two or more jets,  $t\bar{t}$  and single  $t$  production are a significant background. We apply cuts using the number of leptons and jets with  $E_T > 10$  to reduce this background. Our lepton identification is very loose and is described in Ref. [3]. The complete list of cuts is presented in Table I. We define our signal sample (used in extracting the diboson signal) as events in the 40 GeV  $< m_{jj} < 160$  GeV region. We split the signal sample into two sub-samples: one with two  $b$ -tagged jets, and the rest. We use a new  $b$ -tagging algorithm that is described in Sec III. We remove cosmic rays based on timing information from the electromagnetic and hadronic calorimeters.

After this selection, we have four major classes of backgrounds.

1. Electroweak (EWK):  $V$  boson+jet processes that pass our selection requirements. They are estimated using Monte Carlo calculations. We cross-check the estimate using  $\gamma$ +jets data set. This cross-check is described in Sec. V.
2. Multijet: these are events with generic QCD jet production which result in  $\cancel{E}_T$  due to mismeasurements of the jet's momenta. This background is evaluated using a data-driven method. See Sec VI for more details.
3. Top quark production, both singly and in pairs. We estimate this background using a Monte Carlo calculation.
4.  $WW$  production. This is indistinguishable from the signal in the non- $b$ -tagged region. This background is evaluated using a Monte Carlo calculation.

A full list of background estimates is shown in Tab. II.

We use data corresponding to an integrated luminosity of 5.2/fb, collected between December 2004 and February 2010. All data must be certified good for calorimeter and inner tracking (silicon) detectors. Background estimates are derived from Monte Carlo calculations using a combination of PYTHIA [5] and ALPGEN [6], with the geometric and kinematic acceptance obtained using a GEANT-based simulation of the CDF II detector [4]. We use the CTEQ61M parton distribution functions to model the momentum distribution of the initial-state partons [7].

The final number of events is extracted by a fit to the di-jet invariant mass distribution. We split the data into those with two tagged  $b$  quark jets and the rest, and perform a simultaneous fit to the region 40 GeV  $< m_{jj} < 160$  GeV. The fit is described in more detail in Sec. VII.

---

<sup>1</sup> All jets in the region  $|\eta| < 3.6$  are considered.

Variable	Cut value
$\cancel{E}_T$	$> 50 \text{ GeV}$
Jet $E_T$	$> 20 \text{ GeV}$
Jet EM fraction	$< 0.9$
Jet $ \eta $	$< 2$
$\cancel{E}_T$ -significance (signed)	$> 4$
$\min(\Delta\phi(\cancel{E}_T, \text{jet}))$	$> 0.4$
$E_{EM}/E_{TOT}$	$< 0.85$
$E_{EM}/E_{TOT}$	$> 0.3$
$N_{\text{ele}}$	$< 2$
$N_{\text{mu}}$	$< 2$
$N_{\text{ele}} + N_{\text{mu}}$	$< 2$
$N_{\text{jets}, E_T > 10} + N_{\text{ele}} + N_{\text{mu}}$	$< 4$

TABLE I. Complete event selection.

Process(es)	Expected $N_{\text{events}}$ No-tag channel	Expected $N_{\text{events}}$ two-tag channel
EWK	150 000	714
$t\bar{t}$ and single $t$	1 640	374
Multijet Background (QCD)	73 800	58.4
$WW$	2 680	6.8
$WZ/ZZ$	1 150	45.0
$WZ (b\bar{b})$	815 (58.0)	23.8 (20.6)
$ZZ (b\bar{b})$	332 (50.2)	21.2 (19.6)

TABLE II. Background expectations in the no-tag and two-tag channels.  $WZ (b\bar{b})$  and  $ZZ (b\bar{b})$  refer to those diboson decays with  $b$  quark pairs.

### III. $b$ TAGGING

In order to enhance the  $b$ -quark content of our jet sample, we employ a multivariate, neural-network based tagger that provides an output value that serves as a figure of merit to indicate how  $b$ -like a jet appears to be. The tagger used in this analysis is unique in its emphasis on studying individual tracks for characteristics indicating they may have come from a  $B$ -hadron decay. The tagger identifies tracks with transverse momentum  $p_T > 0.4 \text{ GeV}$  which have registered hits in the innermost (silicon) tracking layers, and uses a track-by-track neural network to calculate a figure of merit for a given track's "bness", *i.e.*, the likelihood that it comes from the decay of a  $B$  hadron. The algorithm then uses the top five highest bness tracks in conjunction with jet observables such as displacement of secondary vertex to calculate the overall jet's bness. The training for the track-by-track neural network as well as the jet-by-jet network was performed using a PYTHIA  $ZZ$  Monte Carlo sample.

The observables used in the track-by-track neural network are as follows:

- the transverse momentum of the track in the lab frame ( $p_T$ ),
- the transverse momentum of the track with respect to the jet axis ( $p_{\text{perp}}$ ),
- rapidity (with respect to the jet axis),
- $d_0$  (impact parameter) and its uncertainty  $\sigma_{d_0}$ ,
- $z_0$  ( $z$ -distance from the primary vertex) and its uncertainty  $\sigma_{z_0}$ .

With the track-by-track bnesses in hand, we can calculate the jet-by-jet bnesses. The input observables used are as follows:

- top five track bnesses in the jet,
- number of tracks with bness  $> 0$ ,

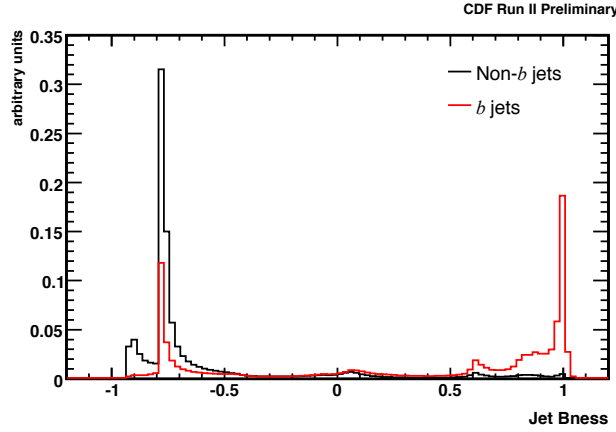


FIG. 1. Jet  $bness$  distribution for jets matched to  $b$  quarks (red) vs. jets not matched to  $b$  quarks (black).

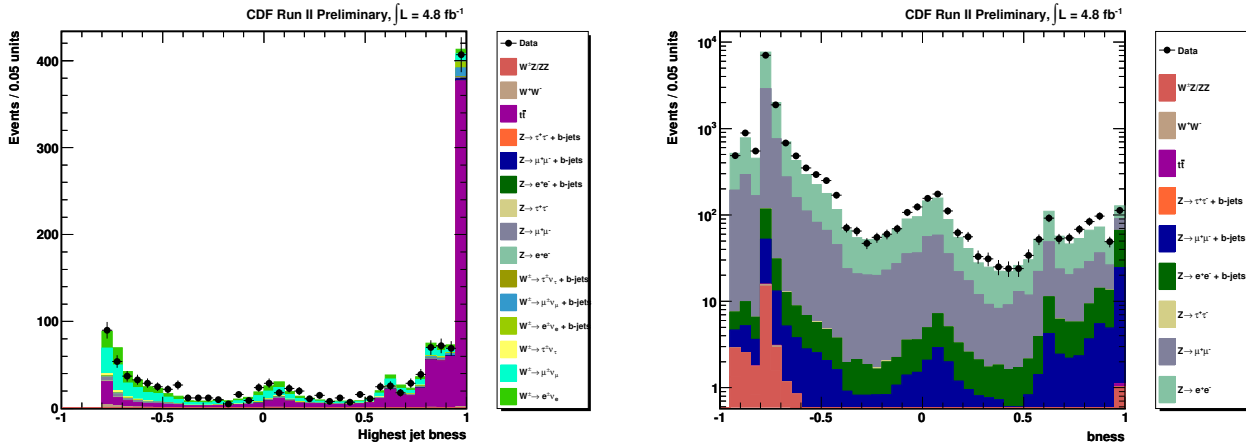


FIG. 2. Shown are two  $b$  tagger validation studies with data. Left: Jet  $bness$  of the highest  $bness$  jet in a  $t\bar{t}$  lepton + jets selection, dominated by heavy flavor. The agreement between data and expectation is quite good, and we see much of the  $b$  enriched samples clustered towards high  $bness$ . Right: A comparison of the jet  $bness$  in data and expectation in the  $Z + 1$  jet selection, dominated by mistags. The agreement between data and MC is good.

- invariant mass of tracks with  $bness > 0$ ,
- the uncertainty on the decay length in the  $xy$  plane ( $\sigma_{L_{xy}}$ ),
- number of  $K_S$  candidates in the jet,
- soft muon tagging information, as described in [8].

Fig. 1 shows the distribution of jet  $bness$  outputs for signal and background ( $b$  jets and light flavor jets). We see good separation between the two types of jets.

In order to verify that the  $b$  tagger response is similar in data and Monte Carlo simulation, we compare data and MC in a  $Z \rightarrow ll + 1$  jet selection, and in a  $t\bar{t}$  (lepton + jets channel) selection. The former offers a comparison of jets that largely do not originate from bottom quarks, while the latter compares jets in a heavily  $b$  enhanced region. Fig. 2 shows the result of this comparison. We use these comparisons to derive a correction to the tagging efficiency and mistag rates in the MC for our jet  $bness$  cuts.

#### IV. TRIGGER AND LUMINOSITY

Our data is triggered on a collection of triggers with missing  $E_T$ . The bulk of the data is collected with a trigger requiring  $\cancel{E}_T > 45$  GeV. Other triggers have a lower  $\cancel{E}_T$  requirement but also include additional requirement on jets in the event or are sometimes prescaled.

We measure the trigger efficiency in a  $Z \rightarrow \mu\mu$  sample. Since the muons are minimum ionizing particles at Tevatron energies, these events appear to have non-zero  $\cancel{E}_T$ .  $Z \rightarrow \mu\mu$  are easy to identify with negligible backgrounds.

We parametrize the trigger efficiency as a function of missing  $E_T$  and also ensure that the trigger does not sculpt the invariant mass distribution  $m_{jj}$  of the jets. The trigger efficiency is parametrized with the functional form

$$\epsilon = \frac{c}{1 + e^{\frac{a-x}{b}}}.$$

The resultant parameterizations are shown in Fig. 3. We see that the trigger does not sculpt the di-jet invariant mass distribution.

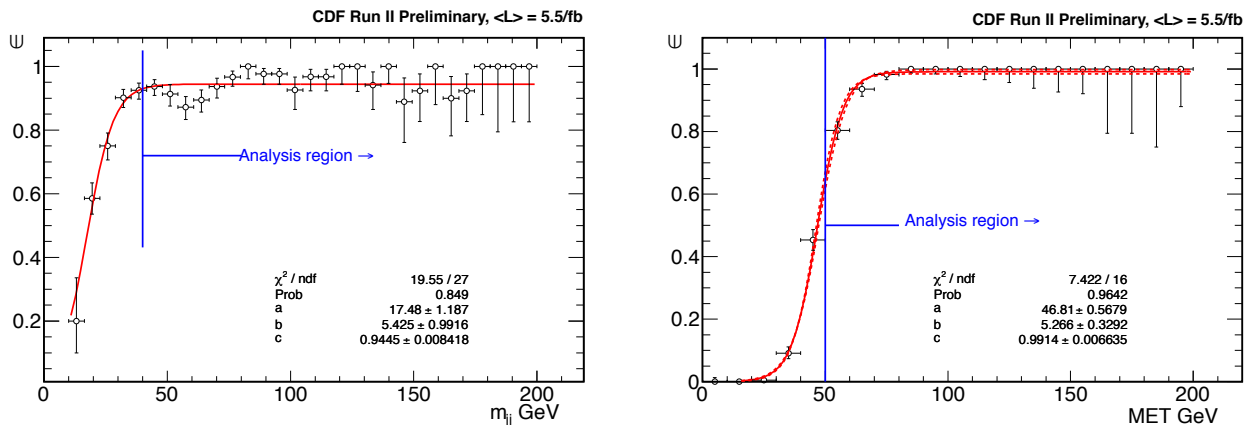


FIG. 3. Trigger efficiency as a function of  $m_{jj}$  (left) and  $\cancel{E}_T$  (right). The dashed lines in the  $\cancel{E}_T$  plot show the statistical uncertainty.

We use  $Z \rightarrow \mu\mu$  events in the high  $p_T$  muon triggered data and  $\cancel{E}_T$  triggered data to establish the product of the luminosity and trigger efficiency of our sample. This effectively does a scaling of the luminosity to a well established standard candle—the  $Z$  cross section—and takes care of the trigger efficiency and prescale factors as well. The effective luminosity of our sample is  $\int \mathcal{L} dt = 5209 \pm 2.2\%(\text{stat}) \pm 6.0\%(\text{lumi})/\text{pb}$ , where the first term comes from the counting uncertainty of the number of detected  $Z \rightarrow \mu\mu$  events and the second term comes from the uncertainty of the luminosity of our reference muon sample.

#### V. $\gamma$ +JETS AS A CROSS-CHECK FOR THE $V$ +JETS SHAPE

We use a  $\gamma$ +jets data sample to check our modeling of the  $V$ +jet background shape. Since our selection has a tight  $\cancel{E}_T$  cut to enhance the sensitivity to the leptonic decays of the  $W$  and  $Z$  ( $\cancel{E}_T > 40$  GeV), we emulate that selection in the  $\gamma$ +jets sample by vectorially adding the photon's  $E_T$  to the measured  $\cancel{E}_T$ . In order to account for any differences in kinematics between  $\gamma$ +jets and  $V$ +jets, we correct the  $\gamma$ +jets data based on the difference between  $\gamma$ +jets and  $V$ +jets Monte Carlo calculations. This way, any production difference is taken into account; however, effects such as detector resolution, PDF uncertainties and ISR/FSR cancel when using  $\gamma$ +jets data. After we apply this correction to the  $\gamma$ +jets data, there is little difference between the photon data and our  $V$ +jets simulation. The templates are shown in Fig. 4. We use the remaining difference determines the systematic uncertainty on the shape of the  $V$ +jets background shape.

#### VI. MULTI-JET BACKGROUND

The multi-jet production does not typically contain large intrinsic  $\cancel{E}_T$ . However, when a jet is not reconstructed accurately the event may acquire large  $\cancel{E}_T$  and pass the analysis selection criteria. This does not happen often, but

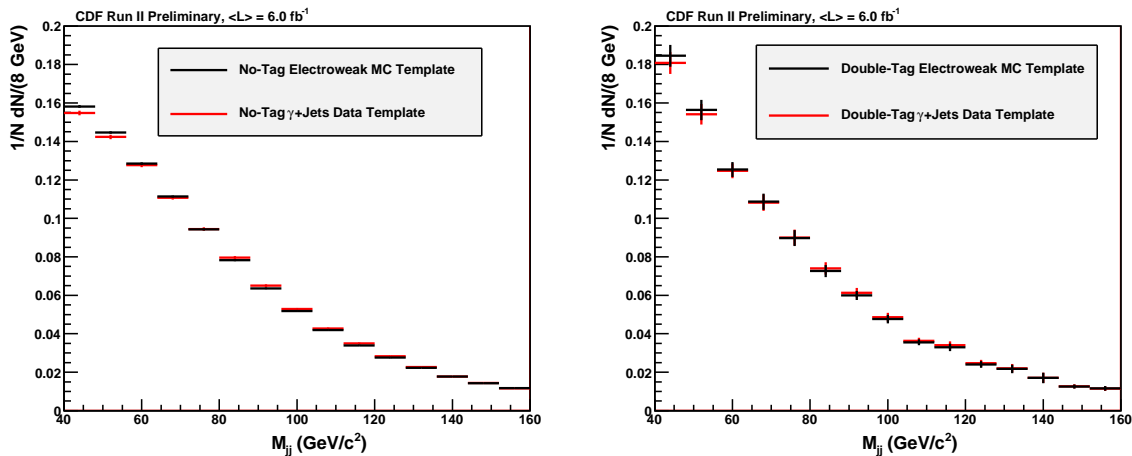


FIG. 4. Comparison of the  $\gamma$ + jets template with the electroweak Monte Carlo-based template in the no-tag (left) and double-tag (right) regions.

because of the high cross section of multi-jet production, it can still be a significant background in a  $\cancel{E}_T$ +jets based analysis. We derive both the initial normalisation and the shape of the multi-jet background from data. The final measure of the amount of multi-jet background will be determined from the extraction fit.

The underlying assumption of how multi-jet background enters the analysis is that either jets are mis-measured, or a leading charged track,  $\pi^0$  or a  $\gamma$  is lost in an uninstrumented region of the detector. We expect the dominant effect to be jet mis-measurement. Most of the multi-jet background is suppressed by the  $\cancel{E}_T$ -significance and  $\min(\Delta\phi(\cancel{E}_T, \text{jet}))$  cuts shown in Fig. 5.

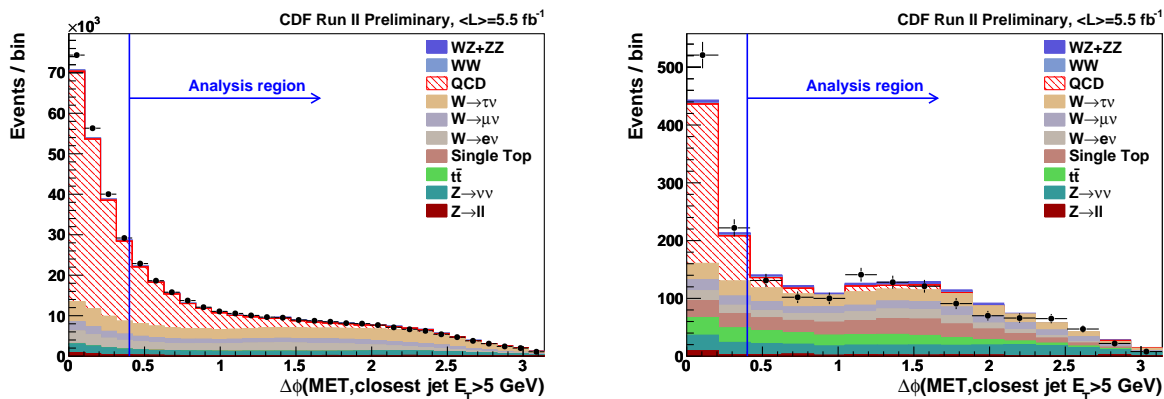


FIG. 5. *Left*: no-tag region. *Right*: 2-tag region. Shown is the minimum azimuthal angular separation  $\min(\Delta\phi(\cancel{E}_T, \text{jet}))$  between all jets with  $E_T > 5$  GeV and the missing  $E_T$ , for events that pass all of the analysis cuts except for the  $\min(\Delta\phi(\cancel{E}_T, \text{jet}))$  cut. The analysis cut is at  $\min(\Delta\phi(\cancel{E}_T, \text{jet})) > 0.4$ .

To estimate the remaining QCD contribution, we construct a new variable,  $\cancel{P}_T$ , to complement the traditional calorimeter based  $\cancel{E}_T$ . The  $\cancel{P}_T$  is defined as the negative vector sum of tracks with  $p_T > 0.3$  GeV/c. Tracks used in the calculation of  $\cancel{P}_T$  have to pass minimal quality requirements and be within a  $\pm 4\sigma$  window in  $z$  (along the beamline) from the primary vertex.

When comparing the azimuth angle ( $\phi$ ) for  $\cancel{E}_T$  and  $\cancel{P}_T$ , we expect the two quantities to align in the case of true  $\cancel{E}_T$  (*e.g.*, for diboson signal and electroweak backgrounds). We will call the difference between these two angles  $\Delta\phi_{MET}$ . Electroweak backgrounds (and diboson signal) will be present in all regions, but will dominate at low  $\Delta\phi_{MET}$  due to the presence of neutrinos. To determine the di-jet mass shape of the multi-jet background, we subtract all other background predictions obtained with Monte Carlo calculations from data, in the multi-jet enhanced region with  $\Delta\phi_{MET} > 1$ . This shape is then scaled up to account for those events with  $\Delta\phi_{MET} \leq 1$ . For the two-tag region, Fig. 6 shows we do not have enough statistics to measure a shape, so we use the same shape as in the no-tag region.

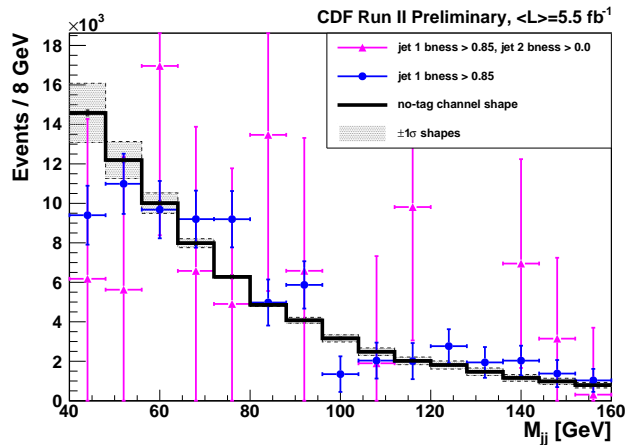


FIG. 6. Multi-jet  $m_{jj}$  shapes obtained for the no-tag channel, 2-tag channel cuts, and intermediate  $b_{\text{ness}}$  cuts, along with the  $\pm 1\sigma$  shapes. The 2-tag and intermediate shapes are normalized to the no-tag shape.

## VII. SIGNAL EXTRACTION AND RESULTS

We extract the number of signal events with a fit to data using the  $CL_s$  method [9]. Histograms for backgrounds and signals are supplied, as well as various systematics as rate and/or shape uncertainties. We perform a simultaneous fit in the two-tag channel and the no-tag channel, with the templates listed below.

- Electroweak background ( $W/Z$ +jets): Normalizations are allowed to float in the fit, as a whole, unconstrained, with no correlation between the two channels.
- $t\bar{t}$  and single top: Gaussian constrained to the theoretical cross sections with uncertainties of 6% and 11%, respectively. We treat these uncertainties as completely correlated, and so they translate to an uncertainty of 7.9% in the no-tag channel and 6.9% in the two-tag channel, due to the relative contributions of each process to the combined top physics template.
- Multi-jet background: Data-driven estimate, Gaussian constrained with an uncertainty of 7% in the no-tag channel and its statistical uncertainty ( $\sqrt{N}/N$ , 13.5%) in the two-tag channel. The uncertainties are treated as uncorrelated.
- $WW$ : We assume that the NLO cross section is correct and apply a Gaussian constraint to the number of  $WW$  events centered on this value with a width of 6%.
- $WZ/ZZ$  signal: As this is our signal, its normalisation is allowed to float unconstrained in the fit.

The systematic errors and their values are shown in Tab. III.

We optimize our selection, in particular for the jet  $b_{\text{ness}}$  thresholds, based on the probability of obtaining a result with significance of  $2\sigma$ . Such scans of the  $b_{\text{ness}}$  parameter space are shown in Fig. 7. The optimization points to a broad region where the sensitivity is maximized and we choose our  $b_{\text{ness}}$  thresholds in that region.

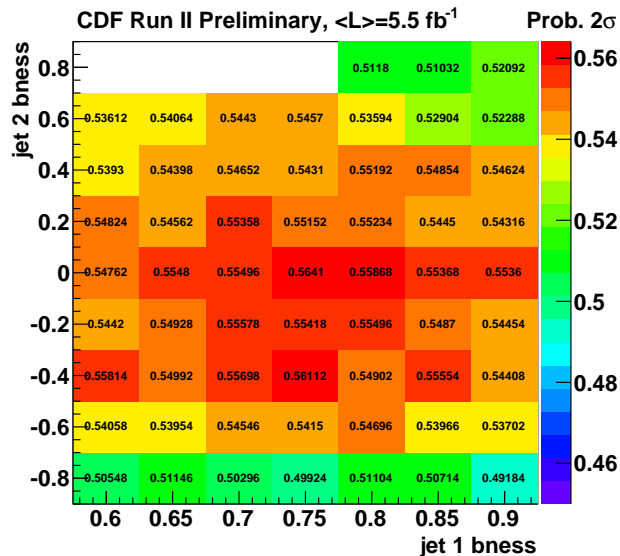
Fig. 8 shows the results of the fit, and Tab. IV. shows the number of fitted events. The  $\Delta\chi^2$  distributions for our null (background-only) and test (signal + background) hypotheses are shown in Fig. 9.

To translate the result of our fit to the data to bounds or limits on the true cross section of  $WZ/ZZ$  production, we construct modified Feldman-Cousins bands by analyzing the distribution of fitted (*i.e.*, measured) cross sections in pseudo-experiments generated with a variety of scale factors on the input signal cross section. The set of input cross sections in our pseudo-experiments range from 0.1 to 3.0 times the standard model value with a step size of 0.1.

For each set of pseudo-experiments, we find a range of measured cross sections that meets a desired coverage threshold. To do this, we first bin the measured scale factors on  $\sigma_{SM}$  in a histogram (100 bins, ranging from 0 to 5). The bin containing the input value of the  $\sigma_{SM}$  scale factor acts as a seed for our coverage interval. We then check the bin contents directly above and below the current interval, and add the most populous one (the one with the highest probability content) to form a new coverage interval, repeating this process until the desired coverage is achieved. Since the fitter cannot return a negative number of fitted signal events, the first bin (at a measured scale factor of 0) may contain a very large number of events; however, we do not treat it differently than any other bin,

Systematic	channel	WZ/ZZ	WW	$t\bar{t}$ & single $t$	EWK	Multijet
Cross Section (Norm.)	no-tag		$\pm 6\%$	$\pm 7.9\%$		$\pm 7\%$
	2-tag		$\pm 6\%$	$\pm 6.9\%$		$\pm 13.5\%$
EWK Shape	both				✓	
Multijet Shape	both					✓
JES Shape/Rate	no-tag	yes/ $\pm 7.1\%$	yes/ $\pm 7.6\%$	no/ $\pm 3.7\%$		
	2-tag	yes/ $\pm 6.9\%$	yes/ $\pm 7.6\%$	no/ $\pm 3.2\%$		
$b$ ness cuts (up)	no-tag	+0.46%	+0.08%	+2.3%		
	2-tag	-13.2%	-23.9%	-12.1%		
$b$ ness cuts (down)	no-tag	-0.51%	-0.08%	-2.7%		
	2-tag	+14.4%	+25.8%	+14.5%		
<b>Acceptance</b>						
JER		$\pm 0.7\%$	$\pm 0.7\%$	$\pm 0.7\%$		
$\cancel{E}_T$ Model		$\pm 1.0\%$	$\pm 1.0\%$	$\pm 1.0\%$		
ISR/FSR		$\pm 2.5\%$	$\pm 2.5\%$	$\pm 2.5\%$		
PDF		$\pm 2\%$	$\pm 2\%$	$\pm 2\%$		
Lumi/Trigger $e$		$\pm 6.4\%$	$\pm 6.4\%$	$\pm 6.4\%$		

TABLE III. Summary of systematic errors considered in our analysis.

FIG. 7. Sensitivity scan for optimizing the  $b$ ness cuts. We plot the probability of a  $2\sigma$  measurement (excluding some systematics), and based on this we place our  $b$ ness cuts at jet 1  $b$ ness  $> 0.85$  and jet 2  $b$ ness  $> 0.0$ .

and if it is included in the range, its entire contents contribute towards the calculation of coverage. This method is a slight variation of the method proposed in [10] due to the strict boundary on the measured scale factors (as well as the input scale factors), but retains the properties that it avoids flip-flopping, and aims for coverage as close as possible to (but always as much as) the stated value.

Figure 10 shows the results of our Feldman-Cousins analysis. Our measured result, using the  $1\sigma$  bands from the modified Feldman-Cousins plot, is then  $\sigma_{measured} = 0.99^{+0.7}_{-0.5} \times \sigma_{SM}$ . In absolute units, we measure

$$\sigma(p\bar{p} \rightarrow WZ, ZZ) = 5.0^{+3.6}_{-2.5} \text{ pb.}$$

We set a limit on  $\sigma_{measured}$  at 13 pb ( $2.5 \times \sigma_{SM}$ ) with 95% CL.

Process(es)	Fit $N_{\text{events}}$ (no-tag)	Fit $N_{\text{events}}$ (2-tag)
EWK	$153300 \pm 3000$	$694 \pm 48$
$t\bar{t}$ and single $t$	$1700 \pm 140$	$313^{+24}_{-26}$
QCD	$72300 \pm 2800$	$54.6 \pm 7.3$
WW	$2720 \pm 190$	$8.3^{+1.8}_{-1.9}$
WZ/ZZ	$1160 \pm 620$	$39.9 \pm 20$

TABLE IV. Fit number of events from the 2-channel fit for WZ/ZZ, with all systematics applied.

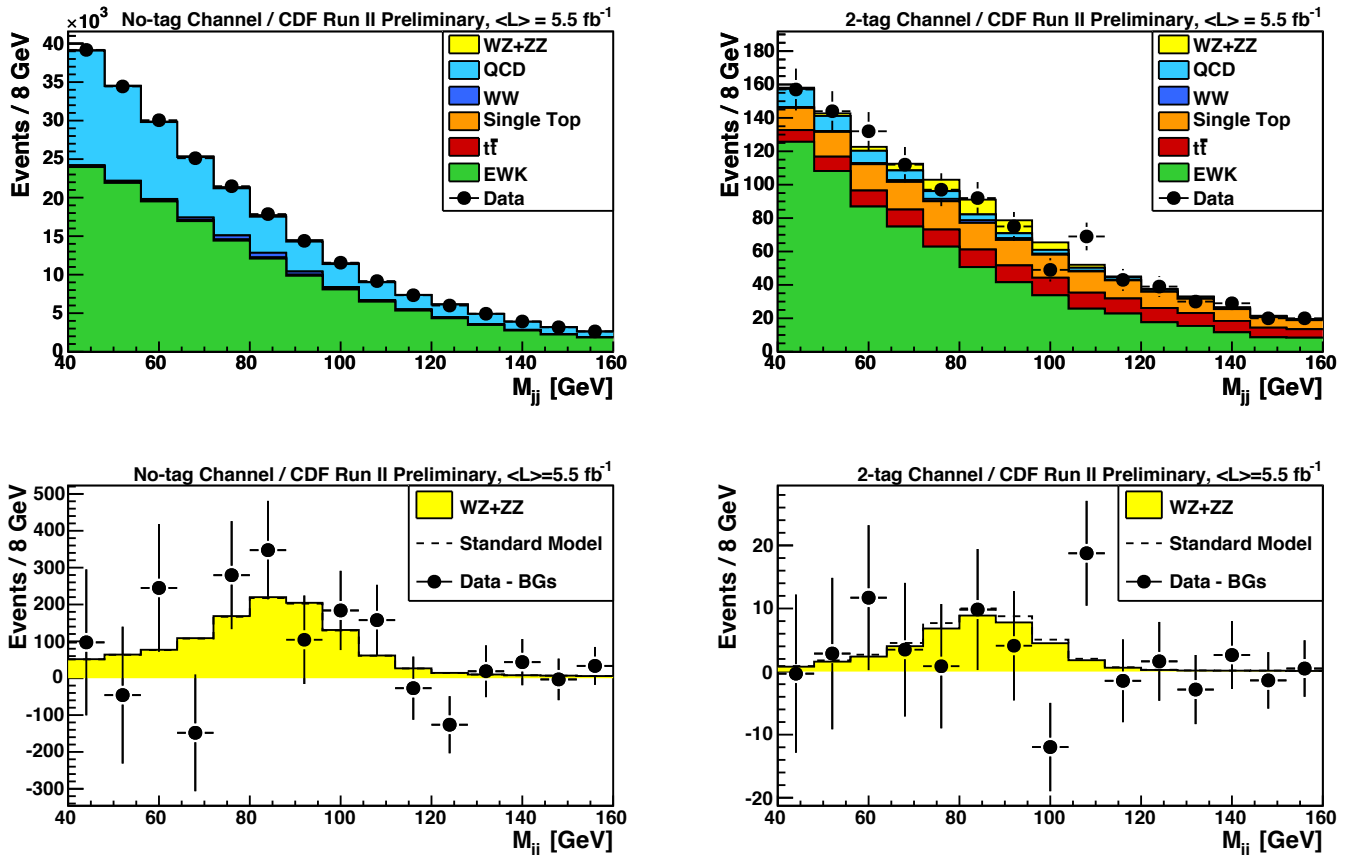


FIG. 8. Result of the fit to data for the double fit to all of WZ/ZZ. Left column is the no-tag channel; right column is the 2-tag channel. Bottom row is data–backgrounds.

## ACKNOWLEDGMENTS

We thank the Fermilab staff and the technical staffs of the participating institutions for their vital contributions. This work was supported by the U.S. Department of Energy and National Science Foundation; the Italian Istituto Nazionale di Fisica Nucleare; the Ministry of Education, Culture, Sports, Science and Technology of Japan; the Natural Sciences and Engineering Research Council of Canada; the National Science Council of the Republic of China; the Swiss National Science Foundation; the A.P. Sloan Foundation; the Bundesministerium für Bildung und Forschung, Germany; the World Class University Program, the National Research Foundation of Korea; the Science and Technology Facilities Council and the Royal Society, UK; the Institut National de Physique Nucleaire et Physique des Particules/CNRS; the Russian Foundation for Basic Research; the Ministerio de Ciencia e Innovación, and Programa Consolider-Ingenio 2010, Spain; the Slovak R&D Agency; and the Academy of Finland.

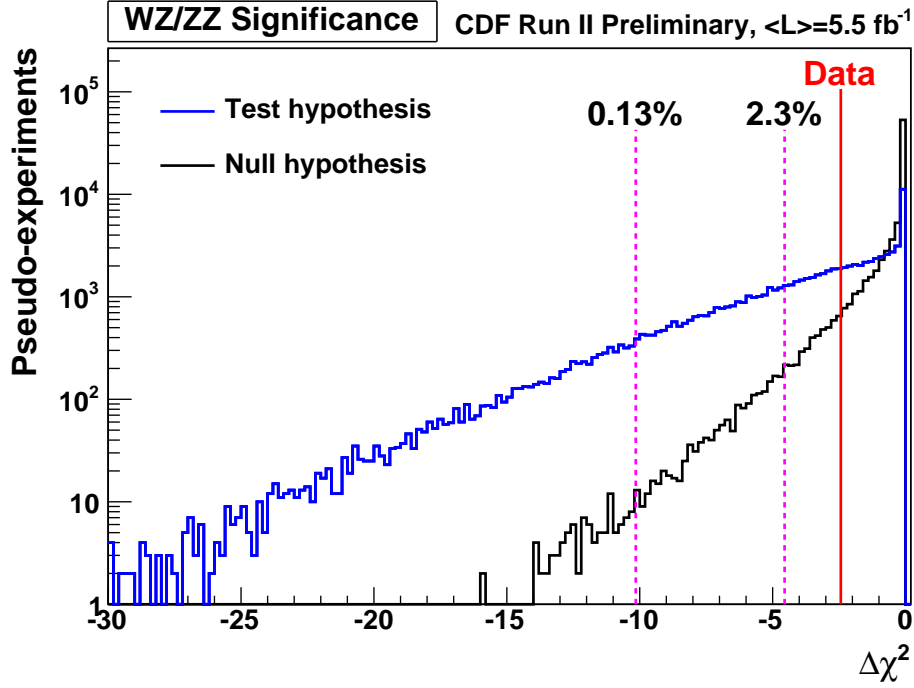


FIG. 9. The  $\Delta\chi^2$  distributions for null and test hypothesis for the double-channel fit to all of  $WZ/ZZ$ . The dashed lines show the  $\Delta\chi^2$  values for which the fraction of the null hypothesis distribution with smaller  $\Delta\chi^2$  is 0.135% and 2.28%. In data,  $\Delta\chi^2 = -2.51$ , and 7.0% of the null hypothesis PEs have a  $\Delta\chi^2$  less than this.

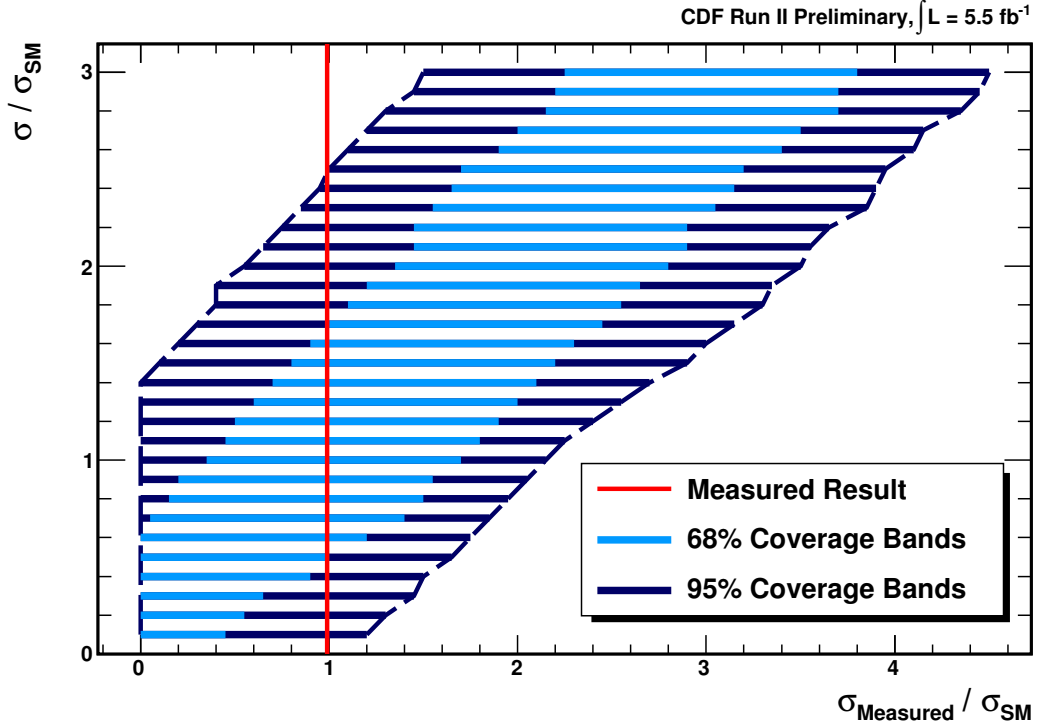


FIG. 10. Confidence bands for the double-channel fit, showing the expected range of measured cross sections as a function of the true cross section, with 68% CL (light blue) and 99% CL (dark blue). Our measured result of  $\sigma(p\bar{p} \rightarrow WZ, ZZ) = 5.0^{+3.6}_{-2.5}$  pb ( $0.99^{+0.7}_{-0.5} \times \sigma_{SM}$ ) (red) corresponds to a 95% CL limit at 13 pb ( $2.5 \times \sigma_{SM}$ ).

- 
- [1] T. Aaltonen *et al.* (CDF Collaboration), Phys. Rev. Lett. **103**, 091803 (2009), arXiv:0905.4714.
  - [2] M. Goncharov *et al.*, Nucl. Instrum. Methods Phys. Res., Sect. A **565**, 543 (2006).
  - [3] Z. Alawi, W. Ketchum *et al.*, *Search for diboson production in the  $ll+jets$  channel*, CDF note 10061.
  - [4] R. Brun *et al.*, CERN Report No. CERN-DD-78-2-REV (unpublished).
  - [5] T. Sjöstrand *et al.*, J. High Energy Phys. **0605**, 026 (2006).
  - [6] M. L. Mangano *et al.*, J. High Energy Phys. **07**, 001 (2003).
  - [7] J. Pumplin *et al.*, J. High Energy Phys. **0207**, 012 (2002).
  - [8] T. Aaltonen *et al.* (CDF Collaboration), Phys. Rev. **D** 79, 052007 (2009).
  - [9] T. Junk, Nucl. Instrum. Meth. **A** 434:435-443 (1999), arXiv:hep-ex/9902006v1.
  - [10] Gary J. Feldman and Robert D. Cousins, Phys. Rev. **D** 57, 3873 (1998).